

# Local deformations and incommensurability of high quality epitaxial graphene on a weakly interacting transition metal

Nils Blanc,<sup>1</sup> Johann Coraux,<sup>2,\*</sup> Chi Vo-Van,<sup>2</sup> Alpha T. N'Diaye,<sup>3</sup> Olivier Geaymond,<sup>2</sup> and Gilles Renaud<sup>1</sup>

<sup>1</sup>*CEA-UJF, INAC, SP2M, 17 rue des Martyrs, 38054 Grenoble Cedex 9 – France*

<sup>2</sup>*Institut NEEL, CNRS & Université Joseph Fourier – BP166 – F-38042 Grenoble Cedex 9 – France*

<sup>3</sup>*II. Physikalisches Institut, Universität zu Köln, Zùlpicher Str. 77, 50937 Köln – Germany*

(Dated: October 17, 2019)

We investigate with high resolution the structure of graphene on iridium, which is a model system for graphene weakly interacting with a transition metal substrate. Even the highest quality epitaxial graphene displays tiny imperfections, *i.e.* small biaxial strains, ca. 0.3%, rotations, ca. 0.5°, and shears over distances of ca. 100 nm, and is found incommensurate, as revealed by X-ray diffraction and scanning tunneling microscopy. These structural variations are mostly induced by the increase of the lattice parameter mismatch when cooling down the sample from the graphene preparation temperature to the measurement temperature. Although graphene weakly interacts with iridium, its thermal expansion is found positive, contrary to free-standing graphene. The structure of graphene and its variations are very sensitive to the preparation conditions. All these effects are consistent with initial growth and subsequent pinning of graphene at steps. These structural imperfections may influence the graphenes properties.

## INTRODUCTION

Graphene preparation at the surface of low-carbon solubility metals like Ir,<sup>1</sup> Cu,<sup>2</sup> or Pt<sup>3</sup> is a surface-confined process which stops once the surface is passivated by a full graphene layer. Therefore it is a straightforward route towards the production of large-area, highly conductive graphene electrodes. Not only is the carbon solubility low in the aforementioned metals, but also their interaction with graphene. In particular in the model graphene on Ir(111) system, where graphene was shown to be almost free-standing,<sup>4</sup> some of the longstanding issues in graphene research could recently be addressed, noteworthy the engineering of graphene's Dirac cone via bandgap opening<sup>5,6</sup> or Fermi velocity renormalization,<sup>7</sup> electron confinement in graphene quantum dots,<sup>8–10</sup> or the use of graphene as a weakly-perturbing and protective layer for fragile surface phenomena such as the Rashba-split Ir surface state.<sup>11</sup> The weak interaction of graphene with metals such as Ir, Cu or Pt also has important consequences regarding the structure of graphene. Indeed, graphene domains with different stackings (twins) with respect to the substrate tend to form on these metals, presumably because the formation of each of the domain involves similar energetic costs. This was first observed some decades ago,<sup>12</sup> further addressed in details on Ir,<sup>13,14</sup> and latter on, on Cu,<sup>15,16</sup> and Pt.<sup>17,18</sup> At the boundary between these domains, dislocations (heptagon pentagon pairs) are found.<sup>13</sup> Such structural defects hinder the improvement of graphene's performances,

*e.g.* for electronic transport,<sup>19,20</sup> heat conduction,<sup>21</sup> or mechanical resistance,<sup>22</sup> towards state-of-the-art ones obtained for exfoliated, suspended graphene. Recently, strategies have been developed in order to avoid the formation of grain boundaries, in graphene having single crystalline orientation at the scale of a centimeter.<sup>23,24</sup> Certain defects are on the contrary desirable: some point defects are expected to switch on magnetism in graphene,<sup>25</sup> and inhomogeneous strain fields were shown to induce electronic gap opening.<sup>26</sup> Gaining knowledge about the nature of defects is hence of fundamental importance.

We report here a high resolution investigation of the structural properties in graphene/Ir(111), with the help of X-ray diffraction and scanning tunneling microscopy (STM), which allowed us to unveil small deviations to a perfect graphene lattice and provide insight into the nature of the graphene/metal epitaxy. Preparation conditions preventing the formation of small- and large-angle grain boundaries in graphene<sup>23</sup> were used, leading to a single graphene phase with its high symmetry crystallographic directions parallel to those of the substrate, at least to the accuracy of laboratory probes such as STM and low energy electron diffraction (LEED).

## METHODS

X-ray diffraction with synchrotron light was conducted inside the ultra-high vacuum growth chamber, under grazing incidence to achieve maximum sensitivity to the graphene overlayer; STM was per-

formed in a separate system.<sup>27</sup>

The iridium single crystal polished in a (111) plane, bought from the "Surface Preparation Laboratory", was prepared by repeated cycles of 0.8-1.5 keV  $\text{Ar}^+$  sputtering at room temperature and high temperature flash. In order to improve the crystal mosaic spread and terrace width, flash temperatures as high as 1500°C were employed. Repeated sample annealing at 800°C under  $\text{O}_2$  partial pressures of  $10^{-8}$  mbar, during 2 h, allowed removing carbon incorporated into the sample during high temperature flashes. The sample temperatures was measured with a pyrometer (60°C uncertainties).

Graphene growth was performed by first adsorbing ethylene at room temperature (5 min with a  $10^{-7}$  mbar pressure of ethylene in the chamber), then flashing the sample temperature to 1200°C, and finally decreasing the sample temperature to 800-1000°C and letting in a  $10^{-8}$  mbar pressure of ethylene for 10 min. This is known to yield a single graphene sheet with almost 100% coverage, free of defects such as grain boundaries, with a single crystallographic orientation, at least to the accuracy of STM and LEED. Compared to growth above 1000°C, it also reduces the lattice mismatch between graphene and its substrate at room temperature after growth, and thus limits the density of wrinkles which form upon cooling.

Surface X-ray diffraction (SXRD) was performed at the INS instrument installed at the BM32 beamline of the European Synchrotron Radiation Facility (Grenoble, France), in a ultra-high vacuum system coupled to a Z-axis diffractometer and with a base pressure below  $10^{-10}$  mbar. Several experiments were performed with a monochromatic photon beam of either 11 and 21 keV incident under angles of 0.38 and 0.19° respectively. The corresponding X-ray attenuation length for Ir is 57 Å at 11 keV, and 68 Å at 21 keV. The incident beam was doubly focused to a size of  $0.4 \times 0.3 \text{ mm}^2$  (full width at half-maximum in horizontal and vertical directions, respectively) at the sample location. Detector slits, located 640 mm away from the sample, were set at 1 mm (or 0.5 mm) parallel to the sample surface (which was vertical) and 8 mm perpendicular to it, resulting in angular acceptances of 0.09° (or 0.045°) in the vertical direction and 0.7° in the horizontal direction. SXRD data were measured with the help of a standard NaI scintillation point detector.

## RESULTS AND DISCUSSIONS

The room temperature (RT) lattice parameter of isolated graphene –a conceptual object– was calculated to be  $a_{\text{C,RT}} = 2.4565 \text{ Å}$ .<sup>28</sup> This is several percents larger than the lattice parameter of most dense-packed transition metal surfaces, a mismatch which cannot be accommodated by graphene presumably due to its high stiffness.<sup>29</sup> So-called moirés having a few nanometer period result. These moirés proved especially sensitive to small displacements and rotations of the graphene lattice as they magnify them by a ca. 10-fold factor.<sup>13</sup> The in-plane structure of graphene and the moiré were investigated by exploring an in-plane cut in reciprocal space (Fig. 1a).

At locations where Ir crystal truncation rods (CTRs) or graphene diffraction rods intersect the in-plane cut of the reciprocal space, intensity maxima are found. For the Ir CTR passing through the center ( $\Gamma_{\text{Ir}}^2$ ) of the third Brillouin zone (BZ), the result is shown in Fig. 3a (see Ref. 27 for the second BZ). The Ir(111) single crystal yield sharp contributions reflecting its high quality. Besides the Ir peaks, a graphene contribution is also observed (at  $\Gamma_{\text{C}}^2$ ), whose position yields the RT in-plane projection of the lattice parameter of graphene,  $a_{\parallel} = 2.4543 \pm 0.0005 \text{ Å}$ . This is substantially larger than the value (2.4435 Å) expected for a commensurate phase with 10 graphene cells matching 9 Ir ones. Since nanorippling is expected with a typical amplitude  $s = 0.5 \text{ Å}$  over  $25 \text{ Å}$ ,<sup>4</sup> due to the weak, varying interaction between graphene and Ir as a function of the location in the graphene/Ir moiré, the actual lattice parameter in graphene on Ir ( $a_{\text{C}}$ ) should be slightly larger (see Fig. 2a), typically 0.3% for a sinusoidal height modulation. This yields  $a_{\text{C}} = 2.4617 \text{ Å}$ , which should be considered as an average lattice parameter (see later), and is only 0.2% larger than the  $a_{\text{C,RT}} = 2.4565 \text{ Å}$  value<sup>28</sup> for isolated graphene. This is consistent with the very limited charge transfer between graphene and Ir, typically 0.01 electron or hole per atom.<sup>4</sup> By contrast, a much larger  $a_{\parallel} = 2.4895 \text{ Å}$  value is found in graphene/Ru(0001),<sup>30</sup> yielding  $a_{\text{C}}$  2% larger than  $a_{\text{C,RT}}$  taking nanorippling (sinusoidal,  $s = 1.5 \text{ Å}$  over  $30 \text{ Å}$ , see Ref. 31) into account, consistent with the strong electron doping<sup>31,32</sup> of graphene on Ru.

A moiré peak, labeled  $\Gamma_{\text{m}}^2$  in Fig. 3a, is found halfway between the Ir ( $\Gamma_{\text{Ir}}^2$ ) and graphene ( $\Gamma_{\text{C}}^2$ ) peaks, corresponding to a  $a_{\text{m}} = 25.6 \pm 0.2 \text{ Å}$  period. Higher order moiré peaks, which are revealed by electron diffraction<sup>33</sup> thanks to extreme surface sen-

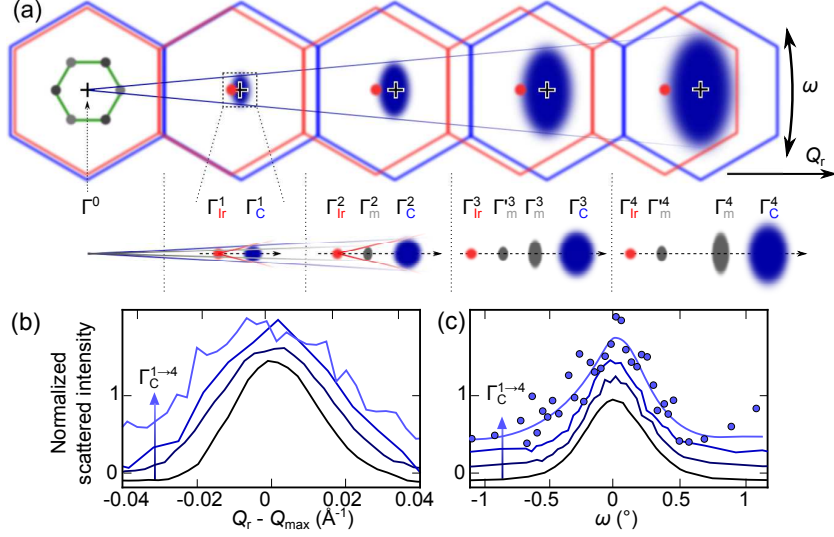


FIG. 1. (Color online) (a) First to fifth graphene BZs and their centers for Ir ( $\Gamma_{\text{Ir}}^{0 \rightarrow 4}$ ) (red) and graphene ( $\Gamma_{\text{C}}^{0 \rightarrow 4}$ ) (blue) where the scattered intensity was measured. Blue ellipses represent in-plane cuts of graphene diffraction rods, characterized by their position, yielding the average projected lattice parameter, as well as by their radial (along the  $Q_r$  direction) and azimuthal (along the  $\omega$  angle) widths. The radial and angular widths are proportional to actual widths obtained after deconvolution from the resolution function. The close-up view marks the measureable moiré diffraction peaks and gives a geometric construction explaining the observed width of the moiré peaks. (b) Radial scans and (c) azimuthal angle scans for graphene at different peak orders ( $\Gamma_{\text{C}}^{1 \rightarrow 4}$ ), vertically shifted for clarity. For  $\Gamma_{\text{C}}^4$ , the azimuthal angle scan (blue disks) has been smoothed (solid lighter blue line) for easing the assessment of the scan FWHM.

sitivity and multiple diffraction, are not detectable around  $\Gamma_{\text{Ir}}^2$ ; however, as sketched in Fig. 1, other first order moiré peaks were measured around  $\Gamma_{\text{Ir}}^3$  and  $\Gamma_{\text{Ir}}^4$ . This agrees with the weak graphene-Ir interaction. These moiré peaks are a signature of local periodic variations of the Ir interatomic distances<sup>34</sup> with the moiré period, as a result of the periodic variation of the metal-graphene interaction induced by the spatially varying proximity of C and Ir atoms. Assuming a small in-plane sinusoidal strain in Ir (sketched in Fig. 2a with a color gradient for Ir atoms), of period  $a_m$  and amplitude  $\varepsilon$ , the position of the  $i$ -th Ir atom in a chain is given by  $a_{\text{Ir}}(i + \varepsilon \cos(2\pi i a_{\text{Ir}}/a_m))$ . Summing up the contribution of all Ir atoms to the scattered amplitude accounts for the observed moiré peaks, whatever the relation, commensurate or not between the Ir, graphene and moiré lattice parameters. Second order commensurability, with 25 graphene unit cells matching 23 metal ones, was concluded for graphene/Ru(0001).<sup>30</sup> The closest high order (second and third) graphene/Ir(111) commensurate structure would consist of 21 graphene unit cells matching 19 metal ones, which is yet slightly off the  $a_m$  and  $a_{\parallel}$  values. We conclude that on the aver-

age, at room temperature, the C and Ir lattices are incommensurate. However, a description in terms of a single incommensurate graphene/Ir(111) phase is too naive as we shall see.

The line-shapes (Fig. 1b) of the graphene in-plane diffraction rods reveal the subtle nature of the graphene-Ir epitaxy. Along the radial direction, the graphene peak width increases linearly with peak order from  $\Gamma_{\text{C}}^1$  to  $\Gamma_{\text{C}}^4$ , in contrast with the  $\Gamma_{\text{Ir}}^{0 \rightarrow 4}$  Ir peaks, whose radial width is constant ( $0.01 \text{ \AA}^{-1}$ ) with order. This radial broadening originates *per se* from in-plane biaxial strains.<sup>35</sup> The most obvious strain pertains to the periodic graphene-Ir interaction. Periodic modulations of in-plane lattice parameter in graphene are indeed expected because the graphene nanorippling induces a periodic variation of the in-plane projection of the carbon bonds (see Fig. 2a). However, these periodic strain fields contribute to the observed satellite (moiré) peaks but do not induce peak broadening.<sup>35</sup> Small random or uncorrelated displacements similar to thermal motion, either static or dynamic, are also excluded as they only yield a Debye-Waller like decrease of the peak height with order, without peak widening.<sup>35</sup>

The peak widening implies either the existence of domains with different average lattice parameters (hereafter referred to as first scenario) or progressive changes of lattice parameter within large domains (hereafter referred to as second scenario).

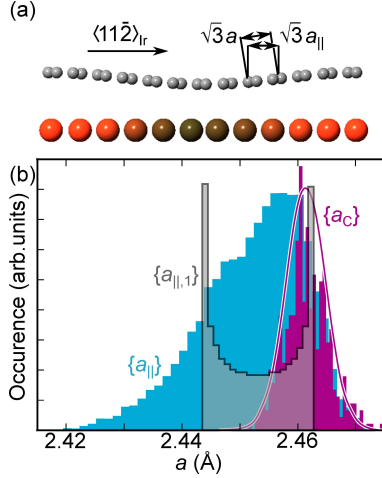


FIG. 2. (Color online) (a) A side-view along a  $\langle 11\bar{2} \rangle_{\text{Ir}}$  direction in Ir illustrating the nanorippling-induced  $\{a_{||,1}\}$  for a given  $a_C$ , and the periodic strain in the last Ir plane (red shades). (b) Distribution  $\{a_C\}$  (purple histogram) of graphene lattice parameters randomly chosen in a standard normal (Gaussian) distribution (as a guide for the eye, the corresponding gaussian function is plotted with a purple line), distribution of in-plane projections,  $\{a_{||,1}\}$  for a given  $a_C$  value (grey histogram), calculated over 10 moiré linear unit cells, and distribution of the projected values,  $\{a_{||}\}$  (cyan histogram), calculated in the same way for all lattice parameters in  $\{a_C\}$ . The width of the  $\{a_C\}$  distribution was chosen to correspond to the increase of the width of the graphene peak as a function of BZ order in the radial direction (Fig. 3b).

The slope of the radial width increase as a function of peak order provides an estimate of the full width at half maximum (FWHM) of the lattice parameter distribution, sketched in Fig. 2b,  $0.0075 \pm 0.002 \text{ \AA}$ . Extrapolation to zero ( $0.011 \text{ \AA}^{-1}$ ) gives (in the first scenario) the typical size of the structurally coherent graphene domains,  $60 \pm 30 \text{ nm}$ . Such domains each having different lattice parameters are sketched in Fig. 4a. Most of these domains should be incommensurate, although high order commensurate phases (*e.g.* with 21 C hexagons coinciding with 19 Ir distances) could also be present in small proportion. The observed linear width increase could alternatively (second scenario) be explained by several 10 nm domains, commensurate, thus

pinned to the Ir(111) lattice, all having the same strain, but separated by domain walls, also called discommensurations.<sup>35</sup> The strain field in these walls fixes their size: the  $0.0075 \text{ \AA}$  FWHM suggests that one (or 1/3 or 2/3 if the domains are located on different terraces) Ir(111) lattice parameter is accommodated in a few 100 graphene unit cells, *i.e.* typically 100 nm (Fig. 4b). Note that detecting such picometric changes of lattice parameters is beyond the possibility of scanning probe microscopy, despite the 10-fold enhancement provided by the moiré, since it would require atomic resolution and distortion-less imaging over several 10 nm. The typical sizes of the graphene domains or domain walls is of the same order of magnitude as the average distance of ca. 100 nm between Ir step edges,<sup>27</sup> as estimated with atomic force microscopy. This may not be fortuitous: Ir step edges, where the interaction between graphene and Ir is expected to be the strongest, could pin the graphene lattice to some extent.

While their radial width increases as a function of peak order, the graphene peaks have constant azimuthal width ( $0.53^\circ$ , much larger than the  $0.08^\circ$  azimuthal width of Ir peaks), as sketched in Fig. 1a and shown in Fig. 1c, which indicates that small-angle disoriented and/or sheared domains are also present. Similar rotations were reported previously, although to a lesser extent ( $0.25^\circ$  FWHM), by a careful inspection of the moiré measured by STM in graphene islands on Ir(111) (Ref. 36) as well as more recently in full layers of graphene on Ru(0001), using low energy electron microscopy and micro-LEED.<sup>37</sup> Such rotations should translate into a ca. 10 times larger rotation of the moiré peak<sup>13</sup> with respect to the nearest Ir peak, *i.e.* into an angular width of the moiré peak with respect to the origin equal to that of the graphene peaks divided by its order (Fig. 1a). The measured  $0.26^\circ$  FWHM of the  $\Gamma_m^2$  moiré peak confirms this interpretation. In the present study, an attempt to further detect lattice variations by STM could only reveal shears, in both graphene and moiré lattices (Fig. 5). Note that the coexistence of different graphene phases was already reported in the case of large-angle orientation variants in graphene/Ir.<sup>14</sup>

In addition to these structural variations, the average epitaxial matching of graphene on Ir(111) was found to depend on preparation conditions, such as the growth temperature ( $T_g$ ). Figure 6a shows a graphene peak (light blue) whose position corresponds to  $a_{||} = 2.4470 \pm 0.0005 \text{ \AA}$ , 0.3% smaller than the previous value. Taking nanorippling into account as before yields  $a_C = 2.4548 \text{ \AA}$ , which is less than 0.1% off the expected value for isolated graphene. The accuracy of our temperature probe



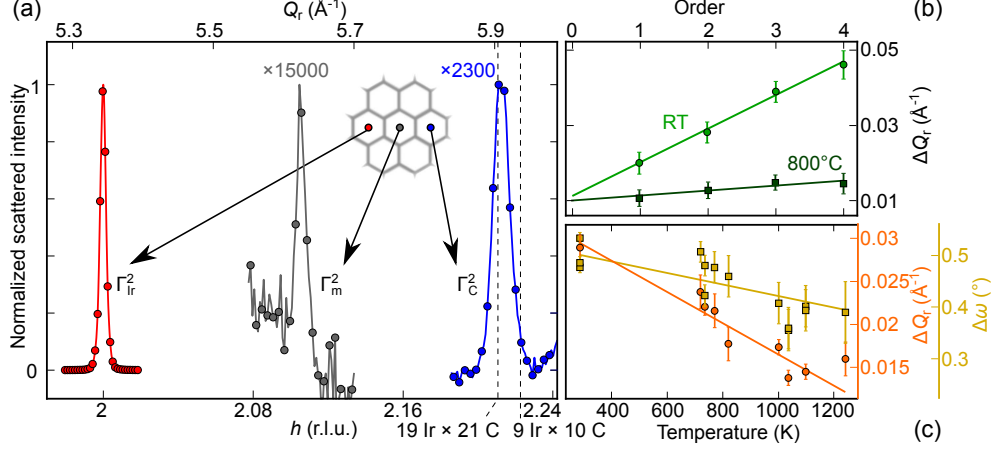


FIG. 3. (Color online) (a) In-plane radial scans at room temperature close to the third BZ center for Ir ( $\Gamma_{\text{Ir}}^2$ ) and graphene ( $\Gamma_{\text{C}}^2$ ) revealing the Ir CTR (red), the graphene rod (blue) and a moiré peak ( $\Gamma_{\text{m}}^2$ , gray), as a function of radial momentum transfer ( $Q_r$ ) and reciprocal space lattice units ( $h$ ). The position of the commensurate structures with 9 Ir cells matching 10 C ones and 19 Ir cells matching 21 C ones are marked. This scan is sensitive only to the in-plane projection of lattice parameters. Due to the hexagonal lattice, the lattice parameter is deduced from the peak position by  $a_{\parallel} = 4\pi/\sqrt{3}Q_r$ . Inset: sketch of the moiré reciprocal lattice. (b) Graphene radial scans FWHMs ( $\Delta Q_r$ ) as a function of peak order ( $\Gamma_{\text{C}}^{0 \rightarrow 4}$ ), at RT and 800°C, and linear fits (lines). (c) Graphene radial ( $\Delta Q_r$ ) and azimuthal ( $\Delta\omega$ ) FWHMs as a function of the sample temperature for the second order peaks. The FWHM shown in (b) and (c) are obtained after deconvolution from the experimental resolution function.

( $\pm 60^\circ\text{C}$ ) does not allow detecting difference in  $T_g$  between the two samples. Actually, the RT graphene lattice  $a_{\parallel}$  parameter was found to vary by almost 0.01 Å for different preparations, with no clear dependence on  $T_g$  (Fig. 6b). The final domain structure and average lattice parameter could be affected by the growth kinetics and substrate defects such as steps or grain boundaries, which might complicate the temperature dependence.

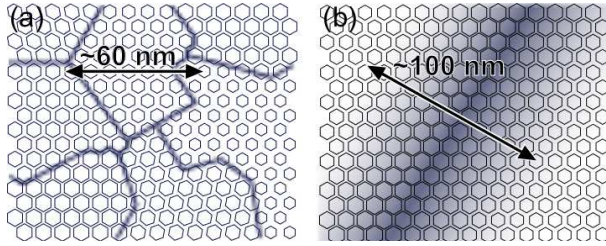


FIG. 4. (Color online) Graphene deformations mapped onto a regular mesh with hexagons at its nodes, whose shapes represent amplified deformations (strain, rotation, shear), for two cases: ca. 60 nm domains, each having distinct lattice parameter (a), and a domain wall (ca. 100 nm) between two domains having the same lattice parameter (b).

Discrepancies were found also in the value of the radial width of the graphene peaks, between two samples tentatively prepared at the same temperature, within the accuracy of the temperature probe. These variations are accounted for in Fig. 3b in the form of error bars. The general trends, namely the slope and the zero-order extrapolation of the radial width linear increase as a function of peak order, do not vary significantly. This implies that the two samples have similar domain size and width of the distribution of graphene lattice parameters. We found no clear dependence of the graphene radial width neither on  $T_g$  nor on  $a_{\parallel}$ , in line with the behavior of  $a_{\parallel}$  versus  $T_g$ .

Besides  $T_g$ , the measurement temperature (following cool down after growth) also influences the epitaxial matching: while between RT and  $800 \pm 60^\circ\text{C}$  the Ir lattice parameter is expanded by 0.48%, for graphene  $a_{\parallel}$  is increased by only 0.33%, from  $2.4470 \pm 0.0005$  to  $2.455 \pm 0.001$  Å (Figs. 6a,b). The thermal expansion coefficient (TEC) of graphene is here found positive, at variance with the vanishing<sup>28</sup> or negative<sup>38</sup> lattice parameter variation predicted for free-standing graphene in this temperature range. The expansion is also much larger than estimated from first principle calculations for graphene/Ir(111).<sup>39</sup> The partial inher-

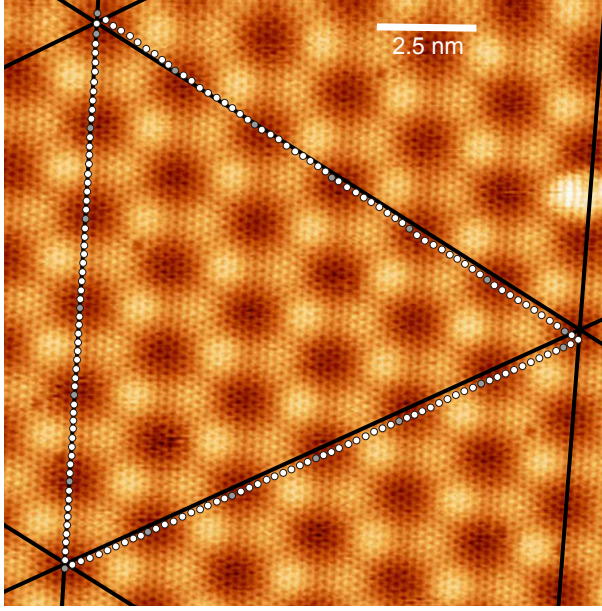


FIG. 5. STM topograph of graphene/Ir(111). Solid lines follow the moiré lattice, white dots mark centers of carbon rings. The two triangles share only one edge, evidencing an in-plane shear.

itance, in graphene, of the Ir TEC, could result from the weak tendency to periodic chemical bonding in graphene/Ir (Ref. 4), or from more subtle effects near steps edges, see below. Although this reminds at first sight the case of the commensurate 13-on-12 superstructure of *h*-BN on Rh(111) (Ref. 40) in which the two TECs are equal, the two TECs are found to differ here,<sup>41</sup> suggesting some slippage of graphene on Ir(111) against temperature-induced stress, presumably due to the high stiffness of graphene. Taking nanorippling into account as before,  $a_C$  is 0.3% larger than the expected lattice parameter ( $a_{800}=2.4556 \text{ \AA}$ ) for isolated graphene at this temperature,<sup>28</sup> while at RT for this sample, the deviation to the expected  $a_{RT}$  value was less than 0.1%. The superperiodicity is slightly decreased, to a value of  $24.5 \pm 0.2 \text{ \AA}$ . The radial scans widths (Fig. 3b) are again found to increase with peak order, but to a much lesser extent than at RT. The corresponding distribution of lattice parameter,  $0.0010 \text{ \AA}$ , is almost one order of magnitude smaller than at RT, but the extrapolation to zero of the radial scans width shows that the size of the structurally coherent graphene domains (in the first scenario) is not significantly changed as compared to the RT value,  $60 \pm 30 \text{ nm}$ . The angular widths are also constant

( $0.43^\circ$ ) as a function of order, but smaller than at RT. Hence, various epitaxial matchings or domain walls are present also in graphene at  $800^\circ\text{C}$ , but they differ from the RT ones in that the associated graphene lattice parameter spread is much smaller. This indicates that the small rotations and biaxial lattice distortions are mostly induced by the increase of lattice parameter mismatch when cooling down the sample from the graphene preparation to the measurement temperature: the larger the mismatch, the larger the structural variations. Analyzing the width of the graphene peaks as a function of sample temperature further supports this view. Figure 3c shows that both the radial and angular widths of a graphene peak increase with decreasing the sample temperature, *i.e.* that graphene minimizes its elastic energy by amplifying the structural variations as the compressive epitaxial stress increases. Such a behavior can be intuited for a lattice whose bonds are more easily rotated than stretched or compressed, as is the case for graphene. The formation of domains with different incommensurate lattice parameters (first scenario, Figure 4a) is however difficult to understand. One might suggest that the balance between flexural modulus, reactivity with Ir (and as a consequence, tendency to accommodate heteroepitaxial stress) and van der Waals interaction with Ir leads to a large number of shallow energy minima with different nanorippling amplitudes, carbon bond lengths, shears, or in-plane orientations, which depend on the domain size and the heteroepitaxial stress. Small graphene nuclei in different metastable states could form in the initial growth stages, then accumulate elastic energy until a critical size, for which forming a domain wall would become favorable. The degree of rotations and strain would depend on the domain size and decrease with decreasing heteroepitaxial stress, *i.e.* with increasing temperature. The fact that no wrinkle is expected, when the temperature differs from  $T_g$  by less than  $400^\circ\text{C}$ ,<sup>42</sup> supports the hypothesis that inhomogeneities develop during growth and subsequent cooling down, and not only upon wrinkle formation. The second scenario (Fig. 4b) could be explained more easily, and is thus favored. Commensurate graphene domains would initiate at step edges, where the interaction of graphene with Ir is expected to be stronger, due to both the bending of graphene over the steps and the high reactivity of Ir atoms at a step edge. However, growing these commensurate domains would cost too high elastic energy with regard to the low interaction with Ir, so that inhomogeneous deformation and shears/rotations resulting in incommensurability between steps are preferred. This would

result in large discommensurations extending over the terraces. The increase of inhomogeneous strain and rotations with decreasing temperature would result naturally from the increasing lattice parameter mismatch with respect to the growth temperature. This scenario would also more easily explain the partial inheritance of the Ir TEC by graphene, as this could result from a complete inheritance in the small commensurate domains near step edges, the weak Ir-graphene interaction resulting in the discommensurations.

## CONCLUSION

The carbon bond length in graphene on Ir(111) is equal to that calculated for isolated graphene to within 0.1%. High resolution X-ray scattering measurements reveal that the graphene and Ir lattices are incommensurate, and that 100 nm domains, limited by the terrace sizes, form upon growth of graphene, with small lattice variations (ca. 0.3%) and rotations (ca. 0.5°). We anticipate that such structural variations may also be encountered in other systems weakly interact-

ing with their substrate, for instance graphene on Cu or dichalcogenates prepared by CVD. The structure of graphene, average lattice parameter, rotations and strain, is found to depend sensitively on temperature, which could allow for epitaxial control of its properties. Further study of these structural variations could make use of the expected resulting particle or quasiparticle scattering, phonon modes, local charge transfers and chemical inhomogeneities, processes which steer many of graphene's properties. Intercalation of species suppressing the non-vanishing graphene-metal interaction, like alkali metals or hydrogen, could yield truly free-standing graphene where the structural inhomogeneities could be released.

## ACKNOWLEDGEMENTS

We thank T. Michely and C. Busse for STM measurements and fruitful discussions. C. V.-V. acknowledges support from the Fondation Nanosciences. Research supported by EU NMP3-SL-2010-246073 "GRENADA" and French ANR ANR-2010-BLAN-1019-NMGEM contracts.

- 
- \* johann.coraux@grenoble.cnrs.fr
- <sup>1</sup> J. Coraux et al., New J. Phys. **11**, 023006 (2009)
  - <sup>2</sup> X. Li et al., Science **324**, 1312 (2009)
  - <sup>3</sup> L. Gao et al., Nature Commun. **3**, 699 (2012)
  - <sup>4</sup> C. Busse et al., Phys. Rev. Lett. **107**, 036101 (2011)
  - <sup>5</sup> I. Pletikosić et al., Phys. Rev. Lett. **102**, 056808 (2009)
  - <sup>6</sup> R. Balog et al., Nature Mater. **9**, 315 (2010)
  - <sup>7</sup> S. Rusponi et al., Phys. Rev. Lett. **105**, 246803 (2010)
  - <sup>8</sup> S.-H. Phark et al., ACS Nano **5**, 8162 (2011)
  - <sup>9</sup> S. K. Hämäläinen et al., Phys. Rev. Lett. **107**, 236803 (2011)
  - <sup>10</sup> D. Subramaniam et al., Phys. Rev. Lett. **108**, 046801 (2012)
  - <sup>11</sup> A. Varykhalov et al., Phys. Rev. Lett. **108**, 066804 (2012)
  - <sup>12</sup> T. A. Land, T. Michely, R. J. Behm, J. C. Hemminger, and G. Comsa, Surf. Sci. **264**, 261 (1992)
  - <sup>13</sup> J. Coraux, A. T. N'Diaye, C. Busse, and T. Michely, Nano Lett. **8**, 565 (2008)
  - <sup>14</sup> E. Loginova, N. Bartelt, P. Feibelman, and K. McCarty, New J. Phys. **11**, 063046 (2009)
  - <sup>15</sup> J. M. Wofford, S. Nie, K. F. McCarty, N. C. Bartelt, and O. D. Dubon, Nano Lett. **10**, 4890 (2010)
  - <sup>16</sup> S. Nie, J. M. Wofford, N. C. Bartelt, O. D. Dubon, and K. F. McCarty, Phys. Rev. B **84**, 155425 (2011)
  - <sup>17</sup> P. Sutter, J. T. Sadowski, and E. Sutter, Phys. Rev. B **80**, 245411 (2009)
  - <sup>18</sup> P. Merino, M. Svec, A. L. Pinardi, G. Otero, and J. A. Martín-Gago, ACS Nano **5**, 5627 (2011)
  - <sup>19</sup> Q. Yu et al., Nature Mater. **10**, 443 (2011)
  - <sup>20</sup> N. Petrone et al., Nano Lett. (2012), :10.1021/nl204481s
  - <sup>21</sup> S. Chen et al., ACS Nano **5**, 321 (2011)
  - <sup>22</sup> C. S. Ruiz-Vargas et al., Nano Lett. **11**, 2259 (2011)
  - <sup>23</sup> R. van Gastel et al., Appl. Phys. Lett. **95**, 121901 (2009)
  - <sup>24</sup> S. Hattab et al., Appl. Phys. Lett. **98**, 141903 (2011)
  - <sup>25</sup> O. V. Yazyev, Phys. Rev. Lett. **101**, 037203 (2008)
  - <sup>26</sup> N. Levy et al., Science **329**, 544 (2010)
  - <sup>27</sup> See supplementary material at [URL will be inserted by AIP] concerning measurement conditions, atomic force microscopy and electron diffraction characterizations of the samples, details about the X-ray data analysis, the effect of Pt cluster grown on graphene, and attempts for measuring higher order moiré peaks.
  - <sup>28</sup> K. V. Zakharchenko, M. I. Katsnelson, and A. Fasolino, Phys. Rev. Lett. **102**, 046808 (2009)
  - <sup>29</sup> C. Lee, X. Wei, J. Kysar, and J. Hone, Science **321**, 385 (2008)
  - <sup>30</sup> D. Martoccia et al., Phys. Rev. Lett. **101**, 126102 (2008)

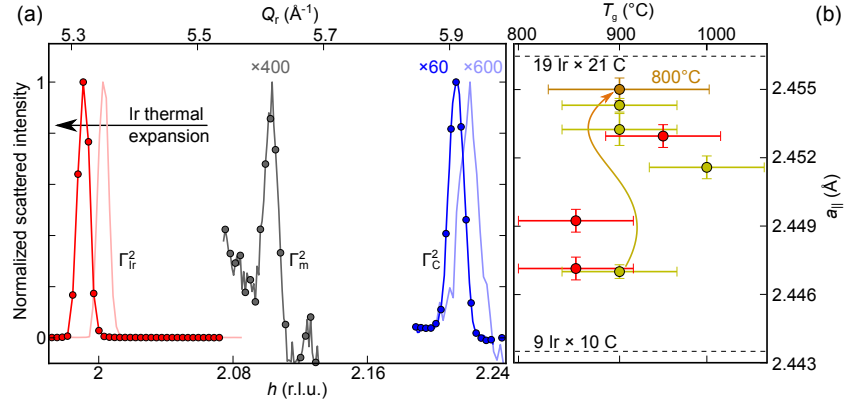


FIG. 6. (a) Radial scans close to the third BZ center at 800°C (light red and light blue), and the same sample at RT (red and blue). Note that the RT measurement corresponds to a sample decorated with Pt clusters, and that Pt clusters do not modify the lattice parameter in graphene while increasing the graphene peak intensity, which allows faster measurements.<sup>27</sup> (b) Spread of in-plane projections,  $a_{||}$ , of  $a_C$ , measured at RT, as a function of the growth temperature  $T_g$ , for two series of measurements (yellow and red data points). The orange point corresponds to a sample grown at 900°C and studied at 800°C.

<sup>31</sup> B. Wang *et al.*, Phys. Chem. Chem. Phys. **10**, 3530 (2008)

<sup>32</sup> P. Sutter, J. Flege, and E. Sutter, Nature Mater. **7**, 406 (2008)

<sup>33</sup> P. Langer *et al.*, New J. Phys. **13**, 053006 (2011)

<sup>34</sup> The periodic modulation of the C-C honeycomb separations also contributes to the moiré peak intensities, but to a much smaller extent, as scattering by C atoms is ca. 40 times smaller than by Ir ones.

<sup>35</sup> A. Guinier, X-ray diffraction in crystals, imperfect crystals, and amorphous bodies (Dover Publications, 1994)

<sup>36</sup> A. T. N'Diaye, J. Coraux, T. N. Plasa, C. Busse, and T. Michely, New J. Phys. **10**, 043033 (2008)

<sup>37</sup> K. L. Man and M. S. Altman, Phys. Rev. B **84**, 235415 (2011)

<sup>38</sup> N. Mounier and N. Marzari, Phys. Rev. B **71**, 205214 (2005)

<sup>39</sup> M. Pozzo *et al.*, Phys. Rev. Lett. **106**, 135501 (2011)

<sup>40</sup> D. Martoccia *et al.*, New J. Phys. **12**, 043028 (2010)

<sup>41</sup> This difference is probably underestimated, graphene probably being flatter at higher temperature due to tensile epitaxial stress, which is known for instance to ~~use monophiles bodies~~ disappear<sup>42</sup>.

<sup>42</sup> A. T. N'Diaye *et al.*, New J. Phys. **11**, 113056 (2009)